Clinical Neurophysiology 156 (2023) 196–206

Contents lists available at ScienceDirect

Clinical Neurophysiology

journal homepage: www.elsevier.com/locate/clinph

Combining ultrasound and microelectrode recordings for postoperative localization of subthalamic electrodes in Parkinson's disease

René Reese [a,*], Thomas Kriesen [b], Maxi Kersten [a,c], Matthias Löhle [a,d], Daniel Cantré [e], Thomas M. Freiman [b], Alexander Storch [a,c,d], Uwe Walter [a,c,d,*]

[a] Department of Neurology, Rostock University Medical Center, Rostock, Germany
[b] Department of Neurosurgery, Rostock University Medical Center, Rostock, Germany
[c] Center for Transdisciplinary Neurosciences Rostock (CTNR), Rostock University Medical Center, Rostock, Germany
[d] German Center for Neurodegenerative Diseases (DZNE) Rostock / Greifswald, Rostock, Germany
[e] Institute of Diagnostic and Interventional Radiology, Pediatric Radiology and Neuroradiology, Rostock University Medical Center, Rostock, Germany

HIGHLIGHTS

- Transcranial sonography reliably determines electrode position in subthalamic nucleus (STN) in relation to ultrasonic landmarks.
- Combining transcranial sonography with intraoperatively obtained microelectrode recording data improves electrode localization.
- Combined ultrasonic and microelectrode recording data support the selection of preferable electrode contact for STN stimulation.

ARTICLE INFO

Article history:
Accepted 1 November 2023
Available online 8 November 2023

Keywords:
Deep brain stimulation
Neuroimaging
Parkinson's disease
Stereotactic neurosurgery
Subthalamic nucleus
Transcranial ultrasound

ABSTRACT

Objective: To assess transcranial sonography (TCS) as stand-alone tool and in combination with microelectrode recordings (MER) as a method for the postoperative localization of deep brain stimulation (DBS) electrodes in the subthalamic nucleus (STN).
Methods: Individual dorsal and ventral boundaries of STN (n = 12) were determined on intraoperative MER. Postoperatively, a standardized TCS protocol was applied to measure medio-lateral, anterior-posterior and rostro-caudal electrode position using visualized reference structures (midline, substantia nigra). TCS and combined TCS-MER data were validated using fusion-imaging and clinical outcome data.
Results: Test-retest reliability of standard TCS measures of electrode position was excellent. Computed tomography and TCS measures of distance between distal electrode contact and midline agreed well (Pearson correlation; $r = 0.86$; $p < 0.001$). Comparing our "gold standard" of rostro-caudal electrode localization relative to STN boundaries, i.e. combining MRI-based stereotaxy and MER data, with the combination of TCS and MER data, the measures differed by 0.32 ± 0.87 (range, −1.35 to 1.25) mm. Combined TCS-MER data identified the clinically preferred electrode contacts for STN-DBS with high accuracy (Cohens kappa, 0.86).
Conclusions: Combined TCS-MER data allow for exact localization of STN-DBS electrodes.
Significance: Our method provides a new option for monitoring of STN-DBS electrode location and guidance of DBS programming in Parkinson's disease.

1. Introduction

Deep brain stimulation (DBS) of the subthalamic nucleus (STN) is highly effective in alleviating motor symptoms and side effects of chronic dopaminergic substitution, thereby improving quality of life in Parkinson's disease (PD) (Deuschl et al., 2006; Weaver et al., 2009). Optimal placement of a DBS electrode with its stimulation contacts in the dorsal (rostral), posterior and lateral part of

* Corresponding authors at: Department of Neurology, Rostock University Medical Center, Gehlsheimer Str. 20, 18147 Rostock, Germany.
E-mail addresses: Rene.Reese@med.uni-rostock.de (R. Reese), Uwe.Walter@med.uni-rostock.de (U. Walter).

https://doi.org/10.1016/j.clinph.2023.11.001
1388-2457/

the STN improves efficacy of STN-DBS in the individual patient (Dembek et al., 2019; Horn et al., 2017; Pozzi et al., 2016; Reese et al., 2012; Wodarg et al., 2012). Preoperative STN target determination on MRI is complicated by common uncertainties in visualization of the STN and its rostral and caudal boundaries (Bus et al., 2018; Güngör et al., 2018; Polanski et al., 2015). Hence, intraoperative microelectrode recordings (MER) are employed to estimate individual functional STN boundaries and intra-STN trajectory lengths, which additionally guide the placement of the permanent electrode (Polanski et al., 2015; Benazzouz et al., 2002; Bjerknes et al., 2018; Steigerwald et al., 2008). Postoperative MRI or CT are performed to exclude intraoperative complications and to verify electrode location. However, the position of the electrode and its stimulation contacts may be distorted by imaging artifacts of the electrode itself (Pinsker et al., 2008) as well as temporary pneumocephalus and brain shift (Saleh et al., 2016). Thus, alternative methods are desirable to localize the electrode in relation to the STN to ensure correct placement and to identify the clinically most effective stimulation contacts.

Transcranial B-mode sonography (TCS) has been proposed as a tool for visualizing the distal metal tip of the electrode for chronic STN-DBS in relation to the echosignals of substantia nigra (SN) (Ispierto et al, 2018; Moringlane et al., 2005; Walter et al., 2011, 2016). While it is difficult on MRI to differentiate STN caudal boundary and SN (Bus et al., 2018; Polanski et al., 2015), TCS can discriminate SN by its, especially in PD, highly echogenic signals (Ahmadi et al., 2020; Becker et al., 1995; Berg et al., 2008). Similar to MRI, however, TCS may not directly visualize the therapeutically most relevant STN area for DBS which is around the rostral boundary of the STN (Milosevic et al., 2020; Zaidel et al., 2010). The postoperative identification of this anatomical key structure and its spatial relation to the position of the stimulation electrode may particularly be helpful in the process of choosing the potentially most effective contact of the electrode for chronic DBS therapy. Such information might reduce programming time usually needed for the separate clinical testing of each contact with respect to symptom alleviation and side effects of DBS (Koeglsperger et al., 2019).

We hypothesized that combining postoperative TCS, assessing the electrode position relative to the SN, with MER data on the rostro-caudal dimension of the STN, once obtained intraoperatively, may allow for precise localization of the DBS electrode relative to STN rostral boundaries in the individual STN at any time point after surgery. In the present study we compare this combined approach (TCS-MER) with our current "gold standard", i.e. the determination of electrode position by intraoperative stereotaxy relative to the MRI-defined stereotactic target point and the rostral STN boundary assessed by MER (stereotaxy-MER). We herewith also validate a standardized approach of TCS determination of STN electrode tip position in relation to the SN.

2. Material and methods

2.1. Participants

Six consecutive PD patients (Table 1), selected for DBS according to established clinical criteria (Fox et al., 2018), gave their written informed consent to participation in this prospective cohort study. The study was approved by the ethical board of the University of Rostock (identifiers A2018-0074, A2013-0005).

2.2. STN target determination, surgical procedure and microelectrode recordings

The terminology of the stereotaxic 3-dimensional coordinate system for DBS refers to dorso-ventral, anterior-posterior, and medial–lateral axis. This corresponds to rostro-caudal, anterior-posterior, and medial–lateral axis in the classical brain anatomy terminology, which is used as a standard in this article. STN target identification and stereotaxic trajectory determination was done on T2-, susceptibility- (SWI), and gadolinium enhanced axial and transversal T1-weighted 3-Tesla MR images with standard coordinates of the STN of 12 mm lateral to the inter-commissural line and 4 mm below and 3 mm behind the mid-commissural point (Reese et al., 2012; Steigerwald et al., 2008). These coordinates were adjusted to the individual MRI anatomy of the STN region to target the rostral, lateral and posterior (motor) part of the STN (Elements, Brainlab AG, Munich, Germany).

On day of surgery, a stereotactic head frame (Leksell Stereotactic System, Elekta Instruments, Stockholm, Sweden) was mounted, followed by a cerebral CT scan to determine individual stereotaxic coordinates of the STN target. Intraoperatively, an array of up to five rigid microelectrodes (FHC Inc., Bowdoin, ME, USA), depending on the individual anatomy, was lowered to 6 mm above the stereotaxic STN target by using the STar Drive Manual System (FHC) in fully awake patients. Patients had been withdrawn from dopaminergic medication for at least 24 h (dopamine agonists 72 h). The central electrode represented the planned trajectory to reach the STN target and was surrounded by up to four additional microelectrodes equally spaced around with center-to-center distance of 2 mm and 90 degrees angle to each other on a virtual circuit (FHC STar Array Locking Carrier). MER (online visual inspection of spiking activity) were done with the Lead Point System (Natus, Middleton, WI, USA) 1 mm stepwise from 6 mm above the stereotactic target point to just below the ventral boundary of the STN. The latter was characterised by reduced background noise without relevant spiking activity, or by signals typical for SN, tonic activity of higher frequency. Entering the STN at its rostral boundary was however characterized by increased background noise and the incidence of phasic and irregular spiking activity (Benazzouz et al. 2002).

MER mapping of the STN region was followed by intraoperative test stimulation to assess DBS clinical efficacy and side effects. The uninsulated tips of the microelectrode guiding tubes ("macroelectrodes") served for monopolar constant current stimulation (Lead Point; 130 Hz frequency, 60 μs impulse width) to test the clinical effects separately per each trajectory. The electrode for chronic stimulation was implanted in the trajectory with optimum results of MER and macroelectrode testing, i.e. an as possible long run through the STN as assessed by MER, contralateral rigidity control and relevantly reduced bradykinesia at low current amplitudes of usually 1.5–2.5 mA, and a sufficient therapeutic window characterized by the occurrence of side effects at amplitudes of at least 3.5 mA or higher. Independent of the manufacturer, the implanted DBS electrodes are equipped with four stimulation ring contacts (each of the two middle ring contacts of the Boston Scientific electrodes consist of three equally segmented elements) with rostral-caudal contact length of 1.5 mm and 0.5 mm isolated interspace. Each electrode was fixed with its two middle contacts in the rostral part of the STN as suggested by MER and verified by intraoperative X-ray. The neurostimulator was implanted on the same day under general anesthesia overlying the pectoralis muscle aponeurosis.

Postoperatively, a cerebral CT was performed within 24hr to exclude intracranial bleeding and to verify correct electrode placement on fusion with preoperative MRI (Elements, Brainlab AG; Fig. 1**A, B**).

2.3. Postoperative assessment of clinical efficacy of STN-DBS

Stimulation parameters and dopaminergic medication were balanced according to the individual needs of the patients. In this study, clinical stimulation efficacy measures obtained at least three

Table 1
Demographic, clinical and stimulation data of the study participants.

Patient	Sex	PD duration [years]	Age at surgery	Daily levodopa equivalent dosage prior to surgery [mg]	Daily levodopa equivalent dosage > 3 months after surgery [mg]	MDS-UPDRS III preoperative Medication ON	MDS-UPDRS III Stimulation OFF / Medication OFF	MDS-UPDRS III Stimulation ON / Medication OFF	Improvement of motor symptoms by STN-DBS, assessed on MDS-UPDRS III [%]	Implanted device	STN-DBS parameters
1	M	7	58	533	283	26	37	24	35	Medtronic Activa RC; electrode model 3389	Left: C + 4-, 2.3 V, 60 µs/130 Hz Right: C + 3-, 1.0 V, 60 µs/130 Hz
2	F	12	60	980	233	18	43	21	51	Boston Scientific Vercise Gevia; electrode model 2201	Left: C + 2-, 3.0 mA, 60 µs/130 Hz Right: C + 3-, 1.5 mA, 60 µs/130 Hz
3	F	9	65	1311	366	11	19	16	16	Medtronic Activa RC; electrode model 3389	Left: C + 3-, 2.5 V, 60 µs/130 Hz Right: C + 3-, 2.4 V, 60 µs/130 Hz
4	M	9	67	1700	999	20	28	16	43	Medtronic Activa RC; electrode model 3389	Left: C + 3-, 1.7 mA, 60 µs/180 Hz Right: C + 4-, 2.2 mA, 60 µs/180 Hz
5	M	6	57	1605	266	16	45	23	49	Boston Scientific Vercise Gevia; electrode model 2201	Left: C + 4-, 1.7 mA, 60 µs/170 Hz Right: C + 4-, 2.2 mA, 60 µs/170 Hz
6	F	8	55	1400	433	5	58	19	67	Boston Scientific Vercise Gevia; electrode model 2201	Left: C + 2-, 1.1 mA, 60 µs/130 Hz Right: C + 2-, 1.1 mA, 60 µs/130 Hz

C denotes case of implanted stimulator (C+, case = anode); 0 to 4, numbered electrode contacts from caudal to rostral (n-, electrode contact = cathode); MDS-UPDRS III, Movement Disorder Society-Sponsored Revision of the Unified Parkinson's Disease Rating Scale, part 3 (motor part); PD, Parkinson's disease; STN-DBS, deep brain stimulation of the subthalamic nucleus.

months after electrode implantation using the MDS-UPDRS part 3 (motor score; off-medication/off-DBS vs. off-medication/on-DBS) were analysed, assuming stable medication and stimulation parameters at this time. Stimulation contact and parameters chosen upon routine clinical criteria were evaluated after 24 h withdrawal of dopaminergic therapy. Additionally, contacts were ranked according to their respective maximum reduction of PD motor symptoms (lateralized MDS-UPDRS motor score items 3–8 and 15–17) due to a stimulation amplitude titrated to 0.5 mA below side effects threshold (pulse width 60 µs, frequency 130 Hz). The contact providing maximum reduction per electrode was named "best contact".

2.4. STN electrode localization by stereotactic coordinates and MER ("gold standard")

Intraoperative MER estimated the rostro-caudal functional boundaries of the STN in the respective trajectory. The implantation depth of the permanent DBS electrode was aligned with the lower end of its most caudal contact (distal metal tip of the electrode) relative to the STN stereotaxic target. The latter was indicated "0mm" with above target values being negative [-] and below target positive [+]. The position of the upper end of the uppermost contact of the DBS electrode relative to the rostral boundary of the STN (motor part; Fig. 2) can thus be estimated by the equation (1):

MER STN rostral boundary (relative to stereotaxic target) [mm] + 7.5 mm (electrode length) – implantation depth (lower end of most caudal electrode contact relative to stereotactic target) [mm].

The MER STN rostral boundary was estimated 0.5 mm above the corresponding recording depth owing to uncertainty of this boundary due to MER recording steps of 1 mm.

2.5. STN electrode localization by combining TCS measures and MER

Postoperative TCS was done by an experienced sonographer (UW) more than three months after DBS surgery at a time of stable DBS parameters and medication, using a high-end ultrasound system (MyLabTwice, Esaote S.p.A., Genova, Italy) equipped with a 2.5-MHz phased-array transducer (PA240). The system settings were as follows: view, 3; size of aperture, 89°; dynamic range, 6; dynamic compression, 2; persist, 7; enhance, 3; density, 2; focuses, 1; gray map, 5; mechanical index, 1.0. For assessing DBS electrode position on TCS we slightly modified our previously reported method (Walter et al., 2011, 2016), as described hereinafter. This results in measuring the shortest rostro-caudal distance from the metal tip of the electrode to the rostral boundary of the SN (directly underneath the caudal boundary of the STN) in virtual extension of the electrode trajectory. First, the ultrasound plane was tilted in a coronal plane to visualize the electrode ipsilateral to insonation in its complete rostral-caudal trajectory relative to the SN (Fig. 1**E,F,H,3A-C**). The SN, situated just caudal to the STN, can be well distinguished from surrounding brainstem structures thanks to its increased echogenicity. Using low amplification of ultrasound to detect the SN echosignals and the DBS electrodes, we regarded the imaging artefact of the distal (caudal) electrode contact, with formerly estimated size of $\leq$ 1 mm (Walter et al., 2011), as negligible and took the distance of the caudal boundary of the most distal electrode contact to the rostral boundary of the SN as it was measured directly on a frozen zoomed TCS image. A location of the distal electrode contact below the rostral boundary of the SN (i.e. typically inside the SN echosignals) resulted in a negative measure (Fig. 3**B**), its location superior to the rostral boundary of the SN in a positive measure (Fig. 3**C**). In the same imaging plane, the medio-lateral position of the most distal

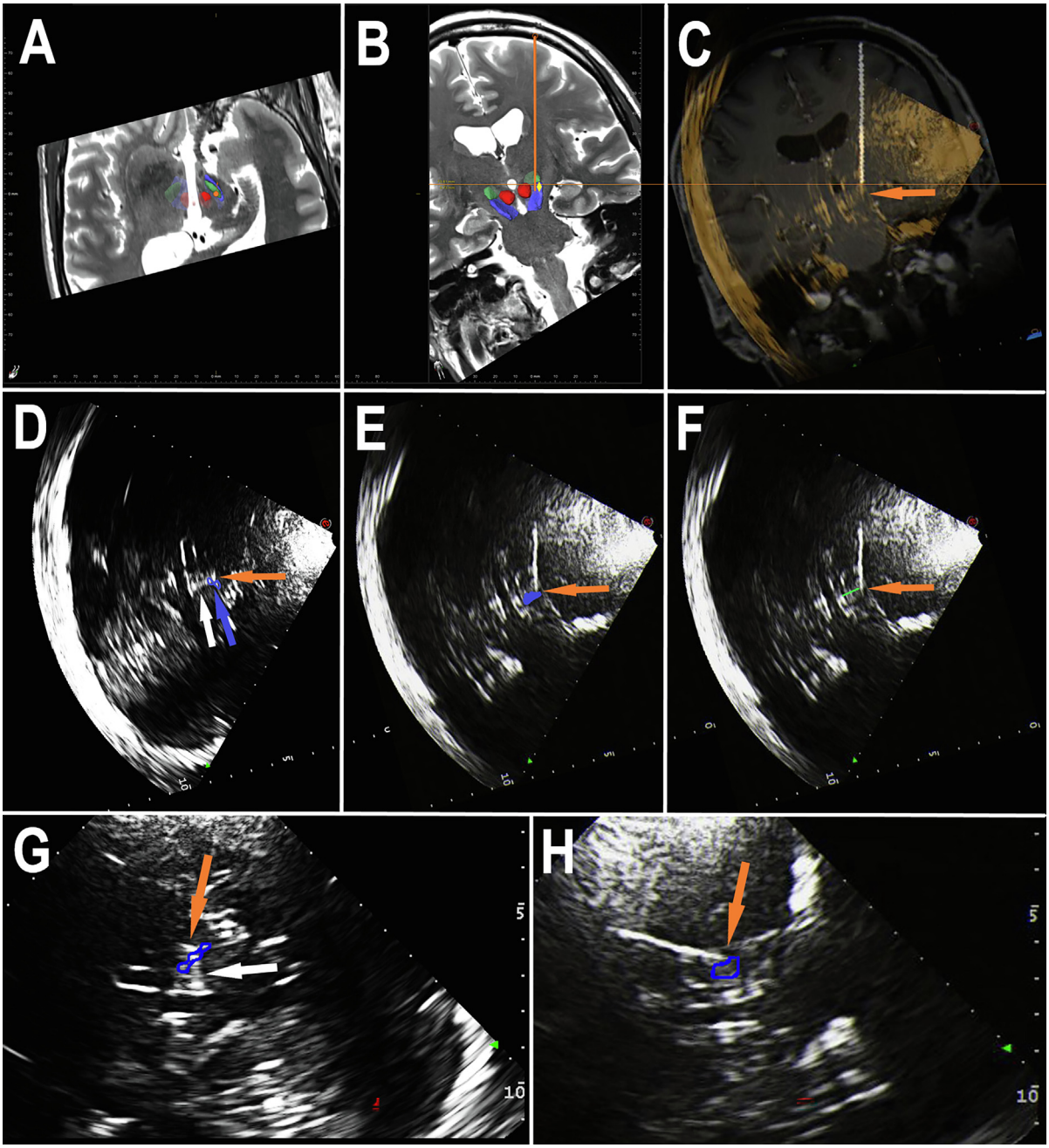

Fig. 1. Comparison of electrode location on transcranial sonography (TCS) versus multimodal neuroimaging. In this patient, the permanent subthalamic nucleus (STN) stimulation electrode was inserted through the central (i.e. the preoperatively planned) trajectory. Images shown in (A)-(F) are scaled according to the electrode position. **A**) Fusion image (Elements, Brainlab) of axial preoperative MRI (STN highlighted in green; substantia nigra [SN], blue; red nucleus, red) with the superimposed electrode position (orange) documented on postoperative CT at the level of the preoperatively planned stereotactic target depth. **B**) Fusion of coronal preoperative MRI (STN, green; SN, blue; red nucleus, red) with the superimposed electrode position (orange) documented on the postoperative CT. Note that the final electrode positioning based on intraoperative recordings was slightly deeper than planned preoperatively, due to the more caudal localization of the STN assessed on intraoperative microelectrode recordings (yellow rhombus). **C**) Postoperative real-time TCS-MRI fusion imaging using the preoperative MRI volume data set with tracing of the planned electrode trajectory (Elements DICOM Burned-In Export, Brainlab). The tip of lowest electrode contact visualized on ultrasound (arrow) is located slightly deeper than planned preoperatively, in agreement with the CT-MRI fusion image (B). **D**) Axial TCS image corresponding to the CT-MRI fusion image (A); orange arrow: transection through electrode; blue arrow: echosignals of SN (surrounded by blue line); white arrow: reverberation artefacts caused by the electrode. **E**, **F**) Coronal TCS image corresponding to the fusion images (B, C); arrow: lower boundary of the lowest electrode contact. SN echosignals are highlighted in blue (E). The distance measure between electrode tip and midline is highlighted in green (F). **G**, **H**) Zoomed TCS images (G: axial, H: coronal) as displayed on the ultrasound monitor, corresponding to images in (D)-(F); orange arrow: tip of the electrode; white arrow: reverberation artefacts caused by the electrode; SN echosignals are surrounded by blue line.

electrode contact was estimated by measuring its distance from midline (mid of 3rd ventricle, cerebral peduncles and/or midbrain raphe). Then, the ultrasound plane was tilted in an axial imaging plane through the midbrain parallel to the orbitomeatal line, again visualizing the distal electrode contact and the SN echosignals (Fig. 1**D,G,3F-H**). In this plane, the anterior-posterior position of the electrode contact was estimated by measuring the distance of the posterior boundary of the distal electrode contact and the anterior boundary of SN echosignals. Again, a location of the distal electrode contact posterior to the anterior boundary of SN

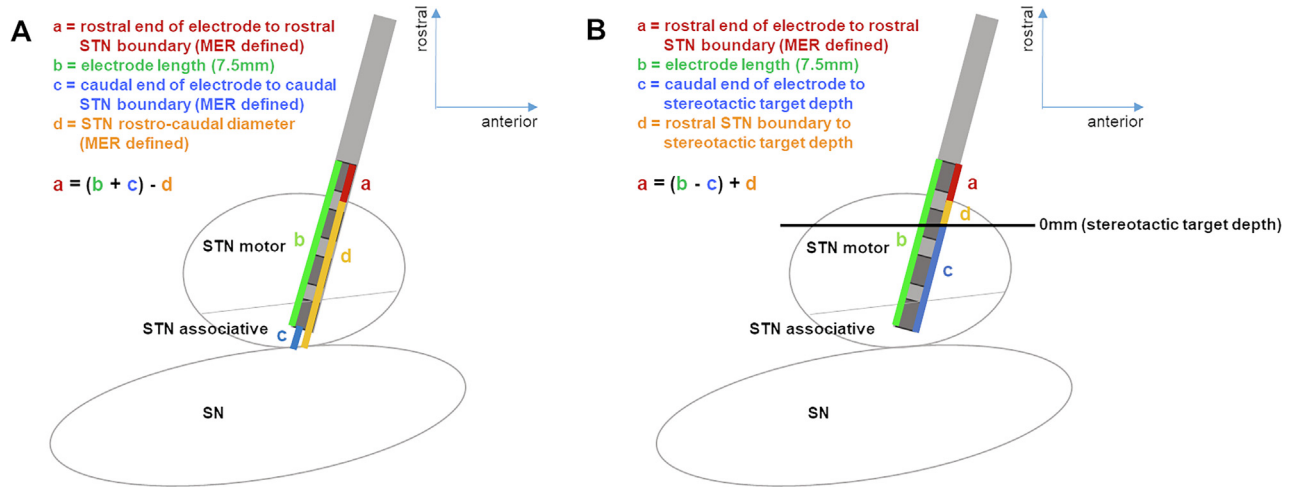

Fig. 2. Sketch of a sagittal view on the localization of an electrode for subthalamic nucleus (STN) stimulation. The electrode is placed in the lateral and dorsal region of the STN with the two middle contacts within the putative motor part of STN. The lowest contact may rather hit the associative part of STN, the limbic part of STN may be represented more medial. The substantia nigra (SN) is located just below the STN. Color lines show relevant measures to capture the permanent electrode location. **A**) Determination of electrode location by combining intraoperative MER and postoperative TCS data: *a* = distance of the upper boundary of the uppermost electrode contact to the upper boundary of the STN defined by MER; *b* = electrode length from the upper boundary of the uppermost contact to the lower boundary of the lowermost contact (here, 7.5 mm, identical for the two electrode models; see Fig. 3D,E); *c* = distance of the lower boundary of the lowermost electrode contact to the upper boundary of the SN assessed on TCS; *d* = rostro-caudal diameter of STN defined by MER. As *b*, *c* and *d* can be measured, *a* can be calculated: a = *(b + c) – d*. Note that for electrodes penetrating the SN, *c* is a negative [-] value. **B**) Determination of electrode location by combining stereotaxy and MER data relative to the STN target depth determined on preoperative MRI ("gold standard"): *a* = distance of the upper boundary of the uppermost contact of the electrode to the upper boundary of the STN defined by MER; *b* = electrode length (7.5 mm); *c* = distance of the lower boundary of the most caudal contact of the electrode to stereotactic target depth; *d* = distance of the upper boundary of the STN defined by MER to stereotactic target depth. We regarded distance measures to target depth (*d*) as being negative [-] if starting rostral to target depth and as being positive [+] if starting below target depth. As *b*, *c* and *d* can be measured, *a* can be calculated: a = *(b – c) + d*.

(i.e. typically inside the SN echosignals) resulted in a negative measure (Fig. 3**G**), and its location anterior to the anterior boundary of SN in a positive measure (Fig. 3**H**). In the same imaging plane, the medial–lateral position of the most distal electrode contact was estimated by measuring its distance from midline; if the referring measures on coronal and axial plane differed, the smaller one was used for further analysis. To evaluate intra-rater reliability, TCS measurements were repeated in all patients (12 electrodes) after 6–8 months by the same investigator blinded to the earlier measures. For assessment of interrater reliability in determining rostro-caudal electrode position TCS was performed by a well-trained second investigator (RR) using in each patient the same, strictly standardized US machine settings. The second investigator had undergone detailed methodological instruction by the experienced TCS investigator (UW) before independently performing the measurements in this study.

The position of the upper end of the uppermost contact of the DBS electrode relative to the rostral boundary of the STN (motor part; Fig. 2) can thus be estimated by the equation (2): 7.5 mm (electrode length) + distance DBS electrode tip to SN [mm] – rostro-caudal extent of the STN on MER [mm].

Again, due to MER recording steps of 1 mm we estimated the STN-MER extent 0.5 mm longer each at rostral and caudal boundaries.

2.6. Comparison of CT and TCS measures of medio-lateral electrode position

Using the postoperative CT data set with a soft tissue kernel, a multi-planar reconstruction with 0.7-mm slice thickness was obtained. The CT windowing level was adapted to an electrode display with nearly their true diameter (1.3 mm). The mid-sagittal plane through the midbrain (aqueduct and midpoint between mammillary bodies/cerebral peduncles) and the coronal plane through the electrodes were used to define the individual midline (Möller et al., 2017) for measurement of its shortest distance from the distal electrode contact per each side. The distance measures obtained on CT were compared with the referring TCS measures

2.7. TCS-MRI real-time fusion imaging of STN electrode position

For real-time TCS-MRI fusion imaging, we used a recalculated pre-operative MRI DICOM data set which included the trace of the planned electrode trajectory with optimized design for TCS-MRI fusion imaging (Elements DICOM Burned-In Export, Brainlab). The fusion imaging was performed using the same ultrasound system (see above), which was additionally equipped with fusion imaging technology (Virtual Navigator, Esaote). The procedures of MRI dataset registration, exact superimposition of MR and TCS images and real-time navigation have been described earlier in detail (Walter et al., 2016). This protocol uses several deep brain structures as reference points and achieves a more precise overlap of TCS and MR image volumes as compared to a skin-surface registration approach (Ahmadi et al., 2015). On the fused image, we compared the planned electrode position (visualized on MRI) with its true postoperative position (visualized on TCS).

2.8. Statistical analysis

Statistical analysis and figure creation were done with GraphPad Prism, version 5.04 (GraphPad Software Inc., San Diego, CA, USA) and SPSS Statistics 27 (IBM, Armonk, NY, USA). The methods to determine the rostro-caudal electrode position (TCS-MER vs. stereotaxy-MER) and the medio-lateral electrode position (TCS vs. CT) were compared with the Pearson correlation test after passing D'Agostino & Pearson omnibus normality test, descriptive statistics and a Bland-Altman plot. Intraclass correlation coefficient (ICC) assessment was used to analyze intrarater (test–retest) and interrater reliability in measuring the distances of lowermost electrode contact from SN echosignals and midline on TCS. Clinical improvement due to STN-DBS, assessed on the MDS-UPDRS motor score in off-DBS and on-DBS states, was analyzed with the Wilcoxon matched-pairs test. The agreement between effective

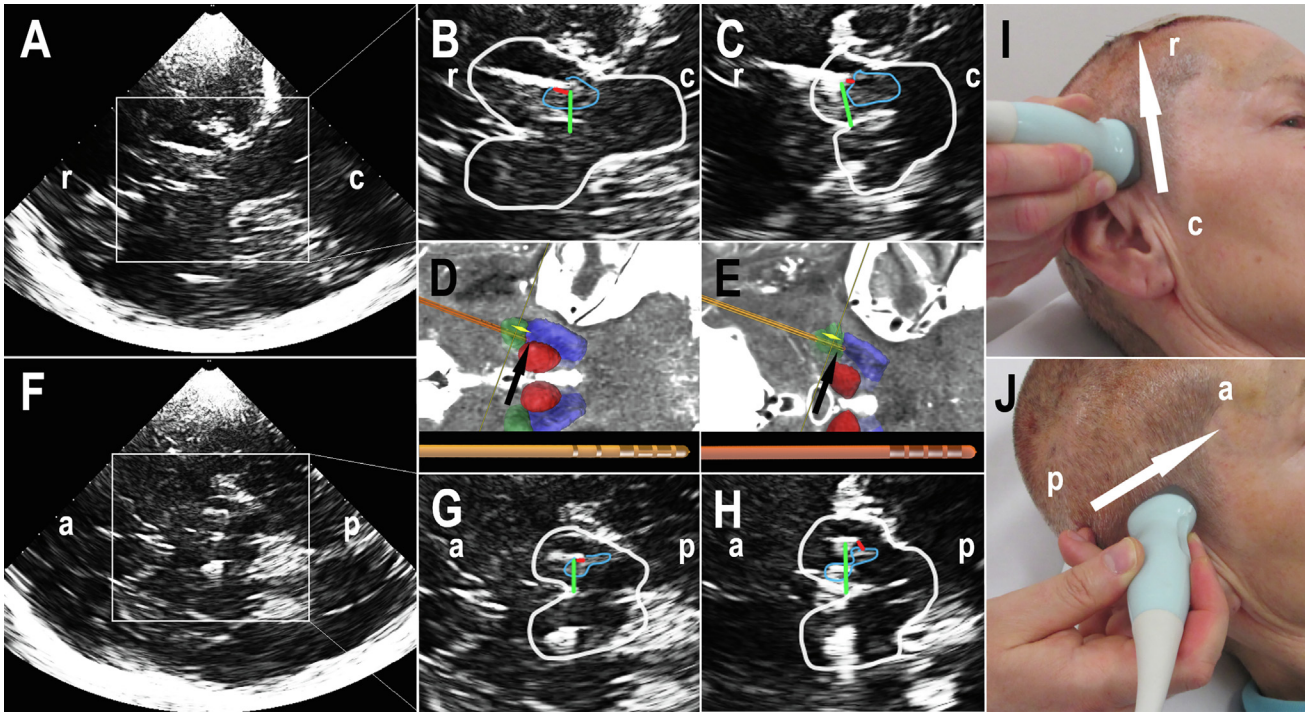

Fig. 3. Assessment of subthalamic nucleus electrode location on transcranial sonography (TCS). a = anterior, c = caudal, p = posterior, r = rostral. **A**) Coronal sonogram through right-sided electrode with visualization of the lower boundary of the lowermost electrode contact inside the substantia nigra (SN) echosignals, which are usually clearly visible in patients with Parkinson's disease. **B**) Zoomed TCS image corresponding to the rectangle in (A). SN echosignals are surrounded by blue line. Red line: distance between the electrode tip and the rostral boundary of SN echosignals (here: −2.0 mm); green line: distance between electrode tip and midline (here: 8.5 mm). **C**) Zoomed TCS image of another patient with the electrode tip located rostrally to the upper boundary of SN echosignals (red line, distance: 0.6 mm). **D**) Fusion image (Elements, Brainlab) of coronal preoperative MRI with the superimposed electrode position documented on the postoperative CT in the same patient as shown in (B). In this electrode (model 2201, Boston Scientific; see insert) the distal contact forms the tip. Note that the CT-MRI fusion image shows the electrode tip (arrow) inside the SN, in agreement with TCS (B). **E**) Coronal CT-MRI fusion image (Elements, Brainlab) in the same patient as shown in (C). In this electrode (model 3389, Medtronic; see insert) the distal electrode contact is distinct from the plastic tip. Note that the CT-MRI fusion image shows the plastic electrode tip inside the SN but the lower boundary of the distal contact (arrow) rostral to the SN, in agreement with TCS (C). **F**) Axial sonogram through right-sided electrode with visualization of the electrode tip inside the SN echosignals. **G**) Zoomed TCS image corresponding to the rectangle in (F). SN echosignals are surrounded by blue line; red line: touching point of the electrode tip at the rostral boundary of SN echosignals (distance: 0 mm); green line: distance between electrode tip and midline (here: 8.5 mm). **H**) Zoomed TCS image of another patient with the electrode tip located anteriorly to the boundary of SN echosignals (red line, distance: 1.3 mm). **I**) Ultrasound transducer position for coronal TCS. **J**) Ultrasound transducer position for axial TCS.

contacts predicted by the TCS-MER method and the clinically most effective contact(s) for STN-DBS per single electrode was tested using Coheńs kappa. P-values < 0.05 were regarded as statistically significant.

3. Results

3.1. Clinical efficacy of STN-DBS

More than three months after electrode implantation, mean stimulation efficacy as assessed on the MDS-UPDRS motor score (off-medication/off-DBS vs. off-medication/on-DBS) was 43.5 % (range: 15.8–67.2 %; Wilcoxon test: p = 0.036) at the stimulation contact and parameters chosen upon clinical criteria (Table 1).

3.2. Test-retest and interrater reliability of TCS measures

Intrarater reliability of the three distance measures (each n = 12) between the lower end of the lowest electrode contact and the reference structure was excellent (rostro-caudal distance to SN echosignal: ICC 0.98 [95 % CI, 0.94–1.0]; anterior-posterior distance to SN echosignal: 0.91 [0.68–0.97]; medio-lateral distance to midline: 0.98 [0.93–1.0]; each p < 0.001; Supplemental Fig. 1). Mean difference between initial and follow-up measures of rostro-caudal lowest contact-to-SN distance was 0.06 ± 0.21 mm (median: 0; range: −0.2 to 0.5 mm), which is far below the length of one electrode contact itself (1.5 mm). Interrater reliability of rostro-caudal lowest contact-to-SN distance was excellent (ICC 0.96 [95 % CI, 0.84–0.99]); mean difference between measures of the two raters was 0.05 ± 0.34 mm (median: 0.1; range: −0.3 to 0.8 mm).

3.3. Comparison of electrode position on planning MRI and postoperative TCS

Real-time TCS-MRI fusion imaging was conducted in a patient in whom the right STN permanent stimulation electrode was, as result of intraoperative testing, inserted through the central (i.e. the pre-operatively planned) trajectory. As a prerequisite, in this case the STN dimension estimated on intraoperative MER corresponded with the STN dimension assessed on the preoperative MRI, which allowed for a direct comparison of the postoperative and the planned electrode position. The postoperative position of the electrode visualized on TCS matched perfectly the planned position highlighted on the superimposed preoperative MR image for anatomical target definition (Fig. 1**C**).

3.4. Comparison of electrode position on postoperative CT-MRI fusion and TCS

Fig. 4 shows the agreement of coronal TCS images of all assessed electrodes and the corresponding preoperative MR images with the respective superimposed electrode position by fusion with the postoperative CT (Elements; Brainlab).

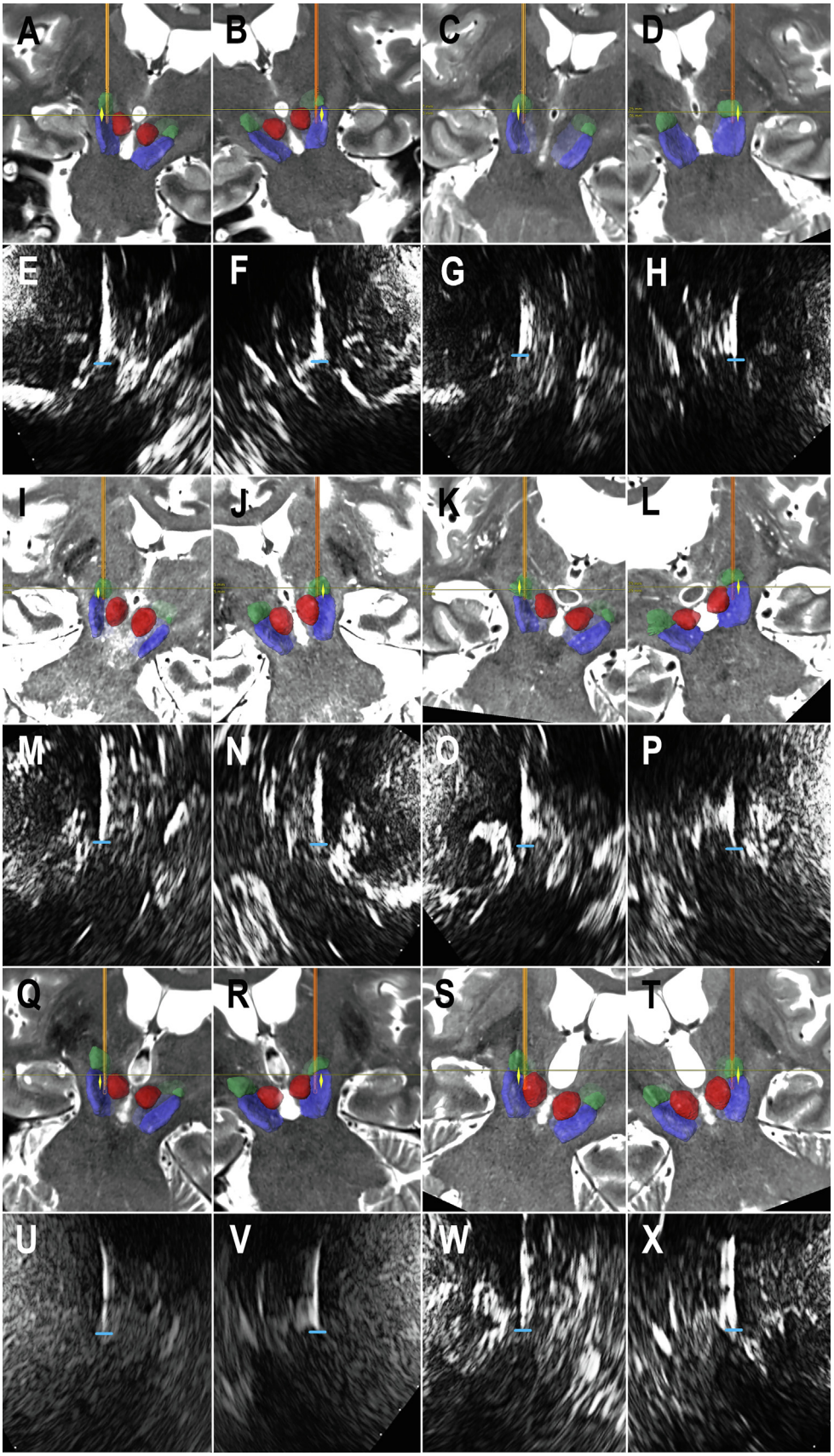
A
B
C
D
E
F
G
H
I
J
K
L
M
N
O
P
Q
R
S
T
U
V
W
X

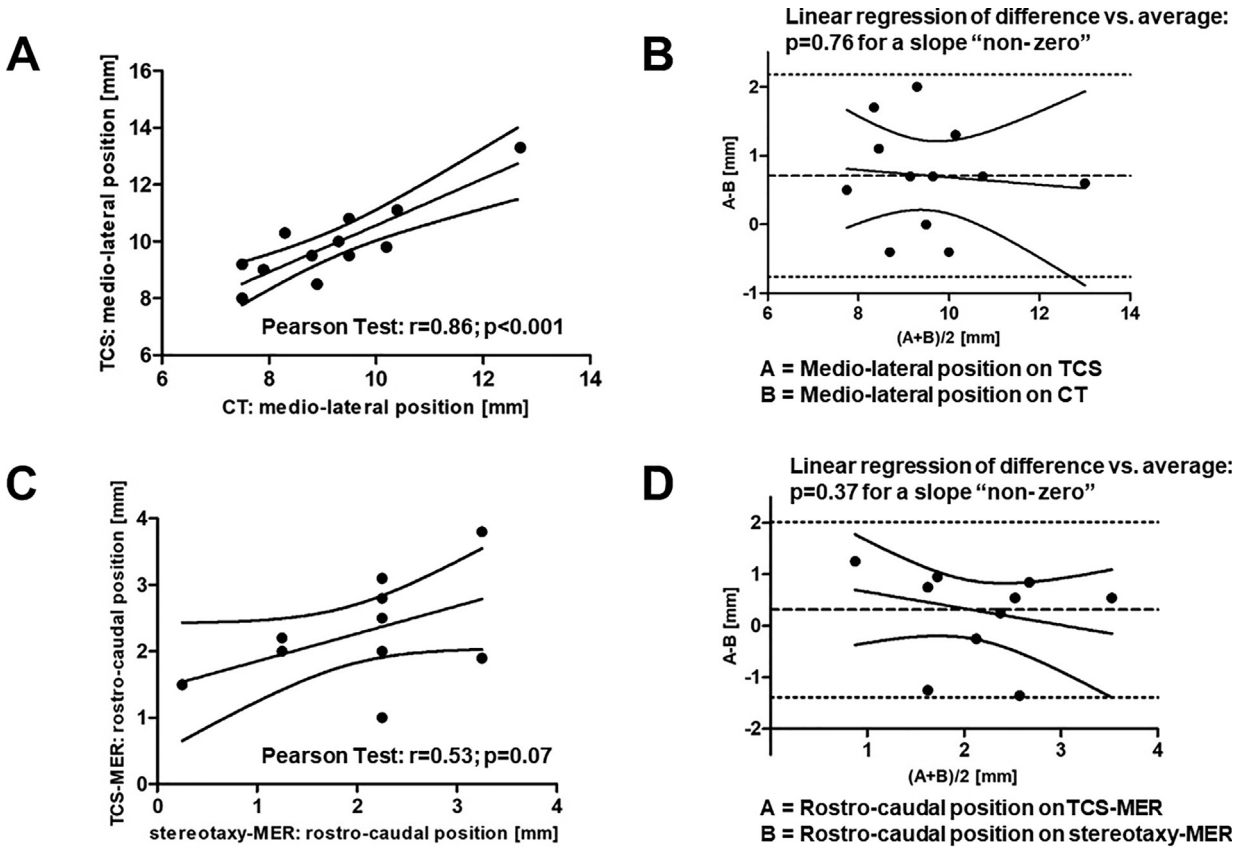

Fig. 5. Comparison of measures of electrode position obtained with 'gold standard' and with transcranial sonography (TCS). **A**) CT and TCS measures of the distance of distal metal electrode tip to midline (medio-lateral position) were highly correlated. **B**) The corresponding Bland-Altman plot visualizes the differences between measures "A" (TCS) and "B" (CT) against the averages of the two measures (best estimation of the true value, which is unknown). Broken line represents mean of the differences (bias), dotted lines represent the limits of agreement, continuous line represents linear regression of difference versus average. A proportional bias in the data set was excluded (p = 0.76 for a slope "non– zero"). **C**) Stereotaxy-MER and TCS-MER measures of the distance of rostral electrode contact to rostral boundary of STN (rostro-caudal electrode position) correlated by trend. **D**) The corresponding Bland-Altman plot visualizes the differences between measures "A" (TCS-MER) and "B" (stereotaxy-MER) against the averages of the two measures (best estimation of the true value, which is unknown). Broken line represents mean of the differences (bias), dotted lines represent the limits of agreement, continuous line represents linear regression of difference versus average. A proportional bias was excluded (p = 0.37 for a slope "non– zero").

3.5. Comparison of CT and TCS measures of medio-lateral electrode position

High correlation was found between CT and TCS distance measures between the distal electrode contact and midline (Pearson test, r = 0.86, p < 0.001; Fig. 5**A**). The Bland-Altman plot showed neither a proportional bias nor outliers in the data set (Fig. 5**B**).

3.6. Comparison of stereotaxy-MER and TCS-MER measures of rostro-caudal electrode position

Mean rostro-caudal extent of the STN estimated by MER was 5.2 ± 0.7 (median, 5.0; range, 4.0–6.0) mm in the trajectory chosen for implantation of the electrode for chronic DBS. Mean difference between the two methods (stereotaxy-MER vs. TCS-MER) determining the position of the upper end of the uppermost contact of the DBS electrode relative to the rostral boundary of the STN was 0.32 ± 0.87 (median, 0.55; range, −1.35 to 1.25) mm. The measures obtained with the two methods correlated by trend (Pearson test, r = 0.53, p = 0.07) (Fig. 5**C**). Taking into account a contact length of the ring contacts of 1.5 mm, each interspaced by 0.5 mm, 12/12 of the distance measures differed by less than one contact length between the two methods. TCS-MER estimated the electrode positions slightly more cranially (10/12 electrodes). The Bland-Altman plot showed neither a proportional bias nor outliers in the data set (Fig. 5**D**).

Fig. 4. Comparison of transcranial sonography (TCS) and CT-MRI coronal fusion images of permanent right and left electrode position in the subthalamic nucleus (STN) in the six studied patients. All images are scaled and centered according to the position of the lower boundary of the lowest electrode contact; corresponding CT-MRI fusion and TCS images are shown in stacked order. The fusion images (Elements, Brainlab) show the preoperative MRI along with the superimposed electrode position (orange) documented on the postoperative CT. The anatomical structures are highlighted as identified on preoperative MRI (green: STN; blue: substantia nigra; red: red nucleus). The yellow rhombus indicates the STN dimension as assessed on intraoperative microelectrode recordings (MER). Note that in some cases the STN location or diameter measured by MER was different from the STN location visualised on MRI. In the TCS images the position of electrode tip is indicated by a blue bar. Landmark structures visible on TCS (e.g. ventricles, basal cisterns) agree well with their position on the corresponding CT-MRI fusion image.

3.7. Identification of optimum electrode contact for STN-DBS by TCS-MER

In 11 of the 12 STN, one of the two clinically "best contacts" per electrode for DBS (assessed by the respective maximum lateralized reduction in MDS-UPDRS by DBS; see Methods) matched with the contact within the STN proper nearest its rostral boundary as conducted by combined TCS and intraoperative MER ("best contact" vs. TCS-MER; Cohen's kappa, 0.86).

4. Discussion

We here present a combined approach of postoperative TCS, assessing the electrode position relative to the SN, and use of MER data on the rostro-caudal dimension of the STN, once obtained intraoperatively, to reliably estimate the position of the uppermost contact of the DBS electrode relative to the rostral boundary of the STN in an individual patient with PD at any time point after surgery. We demonstrate excellent intra- and inter-rater reliability and a high agreement of TCS measures with multimodal DBS electrode imaging data. TCS, in addition to the MER-obtained data on rostro-caudal STN extent, therefore allows for the repeated monitoring of electrode tip position, and, in case of a neurological deterioration due to slight postoperative electrode position change, the adaptation of electrode contact programming.

Clinical experience suggests that electrodes for STN-DBS should be placed in the lateral and posterior part of the STN and that clinically effective contacts are usually found within the STN proper, near its rostral boundary (Dembek et al., 2019; Horn et al., 2017; Wodarg et al., 2012). The latter is also supported pathophysiologically by site-specifically enhanced synchronized oscillatory neuronal activity in the beta frequency band in Parkinsonian motor-off state, which becomes suppressed by DBS in parallel with relevant reduction of PD motor symptoms (Eusebio et al., 2011; Feldmann et al., 2021; Kühn et al., 2008). The postoperative reliable determination of the rostral STN boundary relative to contacts of the DBS electrode could spare programming time. Indeed, one of the two contacts nearest rostral STN boundary were selected for chronic DBS in each case out of our cohort

Today, there is no method to determine the exact anatomic position of an electrode for DBS therapy inside the STN from imaging data alone. Not only because of imaging artefacts of the DBS leads on MRI (Pinsker et al., 2008), it is difficult to recognize the anatomical variability of the STN and its differentiation from other brainstem nuclei, e.g. SN or red nucleus (Bus et al., 2018; Güngör et al., 2018; Polanski et al., 2015; Reese et al., 2012). TCS visualizes DBS electrodes with smaller imaging artefacts compared to CT or MRI (Walter et al., 2011), and offers a high image resolution of intracranial echogenic structures near the midline, especially in the region of upper brainstem and the basal ganglia (Ahmadi et al., 2020; Walter et al., 2008). Moreover, TCS is non-invasive, tolerates patient's movements, and can be easily repeated, making it an ideal tool for postoperative monitoring of DBS electrode position. TCS cannot discriminate the STN directly, but visualizes the neighboring SN by its high echogenicity, thereby allowing for exact distance measurement between SN and DBS electrode tip in direct extension of its trajectory. Using TCS as a stand-alone tool to discriminate suboptimum from optimum STN electrode location, we have earlier proposed a cut-off value of > 5.0 mm of rostro-caudal distance of electrode tip from SN echosignals (Walter et al., 2011, 2016), based on previously reported sizes of DBS target structures (McClelland 3rd et al., 2005; Richter et al., 2004). This value corresponds well with the rostro-caudal diameter of STN of 5.2 ± 0.7 mm assessed here with MER in the trajectory chosen for chronic STN-DBS. However, we also observed in some cases a deviation of location and size of STN estimated on preoperative MRI from intraoperative MER data (Fig. 4), corroborating previous findings (Hamani et al., 2005). Here, TCS showed an excellent intrarater consistency, similar to earlier data (Walter et al., 2011), with differences far below the length of one contact of the stimulation electrode between two time points. This also holds for our inter-rater measurements. Using the TCS method described here, even a slight displacement of the electrode over time should be detected, which however needs to be validated in a prospective blinded study of a greater cohort.

Using combined TCS and MER data, we likewise found differences in the range of greatest one contact length with the tendency to measure the electrode position slightly more cranial than with our "gold standard" of combining intraoperative MER and the stereotactic target determined on the pre-operative MRI. This might be due to the smaller size of echoic iron-generated artefacts in the rostral SN compared to those in the caudal SN (Ahmadi et al., 2020), leading to a larger measured rostro-caudal distance of the electrode tip relative to the rostral SN on TCS. Accordingly, no proportional bias could be detected demonstrating that the difference between methods showed no tendency to get larger (or smaller) while the average of both methods, the best estimation of the true value, increases. TCS can well be used as stand-alone method at any time point during or after surgery (Moringlane et al., 2005; Walter et al., 2009, 2011, 2016). Nevertheless, it remains to be shown in ongoing studies whether the combined methodology with MER data may also be used intraoperatively or early after surgery at a time when intracranial air and/or postoperative brain shift may distort electrode localization.

Potential limitations of present results are to be considered. First, our study sample is rather small owing to the extended real-time TCS-MRI fusion imaging protocol applied for the methodological validation which was difficult to tolerate by the DBS patients. However, with this we were able to provide detailed imaging data from every single case (Fig. 4) illustrating methodological feasibility and precision in a single patient approach, beyond the presentation of group data. Second, there are several technical and patient-related factors which may limit the utility of our combined methodology. Especially, intraoperative MER must be of reliable technical quality to visually determine STN rostral and caudal boundaries. The location of the DBS electrode on TCS requires sufficient experience of the examiner and an adequate temporal acoustic bone window in the individual patient. Moreover, anatomical variability and variability of iron content of substantia nigra may influence to some degree the exact electrode localization on TCS in some patients. The inability to directly visualize STN on TCS remains an issue, as SN boundaries may extend beyond STN in both anterior-posterior and medial–lateral planes (Bot et al., 2019). A similar objection may even be applied to MER which also implies a clear-cut border between SN and STN, despite their sometimes difficult distinguishability (Valsky et al., 2017). However, the agreement of TCS data with TCS-MRI and CT-MRI fusion-imaging data in the present study supports the use of the rostral boundary of SN echosignals in the electrode trajectory as an imaging correlate of SN-STN border. To achieve high intra- and inter-rater reliability of TCS measures as shown in the present study, strictly standardized US machine settings as well as detailed instruction and training of the sonographer by an experienced TCS investigator are required. CT and MRI data enable comparisons on a group level and across centers which is difficult using combined TCS-MER data. We therefore recommend this method mainly as a postoperative monitoring tool in the follow-up visits of patients. TCS and MER are intended not to replace but complement other neuroimaging methods to localize DBS electrodes, and potentially save avoidable MRI or CT repetitions on a single patient level.

5. Conclusions

Combining postoperative brainstem TCS and intraoperative MER may be regarded as a promising novel, non-invasive and time-saving tool to estimate the electrode position for permanent STN-DBS relative to the rostral boundaries of the nucleus at any time point after surgery. Such patient centered information may be used to prospectively identify stimulation contacts potentially relevant for STN-DBS to spare programming time and to improve STN-DBS clinical efficacy. Moreover, primary or secondary malposition of DBS electrodes might be consistently detected and could help to identify patients who may profit from surgical revision of electrodes.

Acknowledgements

The authors wish to thank the patients for their participation in this study.

Funding

The ultrasound and fusion imaging/virtual navigation system was funded by the European Regional Development Fund (EFRE GHS-15-0017) to UW. This work was supported by the Deutsche Forschungsgemeinschaft (DFG) through the Collaborative Research Centre CRC 1270 "Electrically Active Implants" (DFG; SFB 1270 – 299150580) to AS. MK is supported by the Center for Transdisciplinary Neurosciences Rostock (CTNR), University of Rostock, Germany, through its Clinician-Scientist Program. The authors thank Brainlab AG (Munich, Germany) for providing the Elements DICOM Burned-In Export tool which was customized for TCS-MRI fusion imaging in cooperation with UW. The funding sources had no involvement in the study design; in the collection, analysis and interpretation of data; in the writing of the report; or in the decision to submit the article for publication.

Declaration of Competing Interest

The authors declare no conflict of interest with respect to this work.

Data statement

All data are available from the corresponding authors on reasonable request. The request necessitates that the purpose of data re-analysis is in line with the study aims as approved by the ethics review board (see text) and participants consent. Furthermore, consent to data privacy need to be assured by signing an agreement form accordingly.

Appendix A. Supplementary data

Supplementary data to this article can be found online at https://doi.org/10.1016/j.clinph.2023.11.001.

References

Ahmadi SA, Milletari F, Navab N, Schuberth M, Plate A, Bötzel K. 3D transcranial ultrasound as a novel intra-operative imaging technique for DBS surgery: a feasibility study. Int J Comput Assist Radiol Surg 2015;10:891–900. https://doi.org/10.1007/s11548-015-1191-4.

Ahmadi SA, Bötzel K, Levin J, Maiostre J, Klein T, Wein W, et al. Analyzing the co-localization of substantia nigra hyper-echogenicities and iron accumulation in Parkinson's disease: A multi-modal atlas study with transcranial ultrasound and MRI. Neuroimage Clin 2020;26. https://doi.org/10.1016/j.nicl.2020.102185 102185.

Becker G, Seufert J, Bogdahn U, Reichmann H, Reiners K. Degeneration of substantia nigra in chronic Parkinson's disease visualized by transcranial color-coded real-time sonography. Neurology 1995;45:182–4. https://doi.org/10.1212/wnl.45.1.182.

Benazzouz A, Breit S, Koudsie A, Pollak P, Krack P, Benabid AL. Intraoperative microrecordings of the subthalamic nucleus in Parkinson's disease. Mov Disord 2002;17(Suppl 3):S145–9. https://doi.org/10.1002/mds.10156.

Berg D, Godau J, Walter U. Transcranial sonography in movement disorders. Lancet Neurol 2008;7:1044–55. https://doi.org/10.1016/S1474-4422(08)70239-4.

Bjerknes S, Toft M, Konglund AE, Pham U, Waage TR, Pedersen L, et al. Multiple Microelectrode Recordings in STN-DBS Surgery for Parkinson's Disease: A Randomized Study. Mov Disord Clin Pract 2018;5:296–305. https://doi.org/10.1002/mdc3.12621.

Bot M, Verhagen O, Caan M, Potters WV, Dilai Y, Odekerken VJJ, et al. Defining the Dorsal STN Border Using 7.0-T MRI: A Comparison to Microelectrode Recordings and Lower Field Strength MRI. Stereotact Funct Neurosurg 2019;97:153–9. https://doi.org/10.1159/000500109.

Bus S, van den Munckhof P, Bot M, Pal G, Ouyang B, Sani S, et al. Borders of STN determined by MRI versus the electrophysiological STN. A comparison using intraoperative CT. Acta Neurochir (Wien) 2018;160:373–83. https://doi.org/10.1007/s00701-017-3432-5.

Dembek TA, Roediger J, Horn A, Reker P, Oehrn C, Dafsari HS, et al. Probabilistic sweet spots predict motor outcome for deep brain stimulation in Parkinson disease. Ann Neurol 2019;86:527–38. https://doi.org/10.1002/ana.25567.

Deuschl G, Schade-Brittinger C, Krack P, Volkmann J, Schäfer H, Bötzel K, et al. A randomized trial of deep-brain stimulation for Parkinson's disease. N Engl J Med 2006;355:896–908. https://doi.org/10.1056/NEJMoa060281.

Eusebio A, Thevathasan W, Doyle Gaynor L, Pogosyan A, Bye E, Foltynie T, et al. Deep brain stimulation can suppress pathological synchronisation in parkinsonian patients. J Neurol Neurosurg Psychiatry 2011;82:569–73. https://doi.org/10.1136/jnnp.2010.217489.

Feldmann LK, Neumann WJ, Krause P, Lofredi R, Schneider GH, Kühn AA. Subthalamic beta band suppression reflects effective neuromodulation in chronic recordings. Eur J Neurol 2021;28:2372–7. https://doi.org/10.1111/ene.14801.

Fox SH, Katzenschlager R, Lim SY, Barton B, de Bie RMA, Seppi K, et al. International Parkinson and movement disorder society evidence-based medicine review: Update on treatments for the motor symptoms of Parkinson's disease. Mov Disord 2018;33:1248–66. https://doi.org/10.1002/mds.27372.

Güngör A, Baydın ŞS, Holanda VM, Middlebrooks EH, Isler C, Tugcu B, et al. Microsurgical anatomy of the subthalamic nucleus: correlating fiber dissection results with 3-T magnetic resonance imaging using neuronavigation. J Neurosurg 2018;130:716–32. https://doi.org/10.3171/2017.10.JNS171513.

Hamani C, Richter EO, Andrade-Souza Y, Hutchison W, Saint-Cyr JA, Lozano AM. Correspondence of microelectrode mapping with magnetic resonance imaging for subthalamic nucleus procedures. Surg Neurol 2005;63:249–53. https://doi.org/10.1016/j.surneu.2004.05.036.

Horn A, Neumann WJ, Degen K, Schneider GH, Kühn AA. Toward an electrophysiological "sweet spot" for deep brain stimulation in the subthalamic nucleus. Hum Brain Mapp 2017;38:3377–90. https://doi.org/10.1002/hbm.23594.

Ispierto L, Muñoz J, Cladellas JM, Cuadras P, Capellades J, Latorre P, et al. Post-Operative Localization of Deep Brain Stimulation Electrodes in the Subthalamus Using Transcranial Sonography. Neuromodulation 2018;21:574–81. https://doi.org/10.1111/ner.12733.

Koeglsperger T, Palleis C, Hell F, Mehrkens JH, Bötzel K. Deep Brain Stimulation Programming for Movement Disorders: Current Concepts and Evidence-Based Strategies. Front Neurol 2019;10:410. https://doi.org/10.3389/fneur.2019.00410.

Kühn AA, Kempf F, Brücke C, Gaynor Doyle L, Martinez-Torres I, Pogosyan A, et al. High-frequency stimulation of the subthalamic nucleus suppresses oscillatory beta activity in patients with Parkinson's disease in parallel with improvement in motor performance. J Neurosci 2008;28:6165–73. https://doi.org/10.1523/JNEUROSCI.0282-08.2008.

McClelland 3rd S, Ford B, Senatus PB, Winfield LM, Du YE, Pullman SL, et al. Subthalamic stimulation for Parkinson disease: determination of electrode location necessary for clinical efficacy. Neurosurg Focus 2005;19:E12. https://doi.org/10.3171/foc.2005.19.5.13.

Milosevic L, Scherer M, Cebi I, Guggenberger R, Machetanz K, Naros G, et al. Online Mapping With the Deep Brain Stimulation Lead: A Novel Targeting Tool in Parkinson's Disease. Mov Disord 2020;35:1574–86. https://doi.org/10.1002/mds.28093.

Möller L, Kassubek J, Südmeyer M, Hilker R, Hattingen E, Egger K, et al. Manual MRI morphometry in Parkinsonian syndromes. Mov Disord 2017;32:778–82. https://doi.org/10.1002/mds.26921.

Moringlane JR, Fuss G, Becker G. Peroperative transcranial sonography for electrode placement into the targeted subthalamic nucleus of patients with Parkinson disease: technical note. Surg Neurol 2005;63:66–9. https://doi.org/10.1016/j.surneu.2004.01.029.

Pinsker MO, Herzog J, Falk D, Volkmann J, Deuschl G, Mehdorn M. Accuracy and distortion of deep brain stimulation electrodes on postoperative MRI and CT. Zentralbl Neurochir 2008;69:144–7. https://doi.org/10.1055/s-2008-1077075.

Polanski WH, Martin KD, Engellandt K, von Kummer R, Klingelhoefer L, Fauser M, et al. Accuracy of subthalamic nucleus targeting by T2, FLAIR and SWI-3-Tesla MRI confirmed by microelectrode recordings. Acta Neurochir (Wien) 2015;157:479–86. https://doi.org/10.1007/s00701-014-2328-x.

Pozzi NG, Arnulfo G, Canessa A, Steigerwald F, Nickl R, Homola GA, et al. Distinctive neuronal firing patterns in subterritories of the subthalamic nucleus. Clin Neurophysiol 2016;127:3387–93. https://doi.org/10.1016/j.clinph.2016.09.004.
Reese R, Pinsker MO, Herzog J, Wodarg F, Steigerwald F, Pötter-Nerger M, et al. The atypical subthalamic nucleus–an anatomical variant relevant for stereotactic targeting. Mov Disord 2012;27:544–8. https://doi.org/10.1002/mds.24902.
Richter EO, Hoque T, Halliday W, Lozano AM, Saint-Cyr JA. Determining the position and size of the subthalamic nucleus based on magnetic resonance imaging results in patients with advanced Parkinson disease. J Neurosurg 2004;100:541–6. https://doi.org/10.3171/jns.2004.100.3.0541.
Saleh C, Dooms G, Berthold C, Hertel F. Post-operative imaging in deep brain stimulation: A controversial issue. Neuroradiol J 2016;29:244–9. https://doi.org/10.1177/1971400916639960.
Steigerwald F, Pötter M, Herzog J, Pinsker M, Kopper F, Mehdorn H, et al. Neuronal activity of the human subthalamic nucleus in the parkinsonian and nonparkinsonian state. J Neurophysiol 2008;100:2515–24. https://doi.org/10.1152/jn.90574.2008.
Valsky D, Marmor-Levin O, Deffains M, Eitan R, Blackwell KT, Bergman H, et al. Stop! border ahead: Automatic detection of subthalamic exit during deep brain stimulation surgery. Mov Disord 2017;32:70–9. https://doi.org/10.1002/mds.26806.
Walter U, Kanowski M, Kaufmann J, Grossmann A, Benecke R, Niehaus L. Contemporary ultrasound systems allow high-resolution transcranial imaging of small echogenic deep intracranial structures similarly as MRI: a phantom study. Neuroimage 2008;40:551–8. https://doi.org/10.1016/j.neuroimage.2007.12.019.
Walter U, Wolters A, Wittstock M, Benecke R, Schroeder HW, Müller JU. Deep brain stimulation in dystonia: sonographic monitoring of electrode placement into the globus pallidus internus. Mov Disord 2009;24:1538–41. https://doi.org/10.1002/mds.22663.
Walter U, Kirsch M, Wittstock M, Müller JU, Benecke R, Wolters A. Transcranial sonographic localization of deep brain stimulation electrodes is safe, reliable and predicts clinical outcome. Ultrasound Med Biol 2011;37:1382–91. https://doi.org/10.1016/j.ultrasmedbio.2011.05.017.
Walter U, Müller JU, Rösche J, Kirsch M, Grossmann A, Benecke R, et al. Magnetic resonance-transcranial ultrasound fusion imaging: A novel tool for brain electrode location. Mov Disord 2016;31:302–9. https://doi.org/10.1002/mds.26425.
Weaver FM, Follett K, Stern M, Hur K, Harris C, Marks Jr WJ, et al. Bilateral deep brain stimulation vs best medical therapy for patients with advanced Parkinson disease: a randomized controlled trial. JAMA 2009;301:63–73. https://doi.org/10.1001/jama.2008.929.
Wodarg F, Herzog J, Reese R, Falk D, Pinsker MO, Steigerwald F, et al. Stimulation site within the MRI-defined STN predicts postoperative motor outcome. Mov Disord 2012;27:874–9. https://doi.org/10.1002/mds.25006.
Zaidel A, Spivak A, Grieb B, Bergman H, Israel Z. Subthalamic span of beta oscillations predicts deep brain stimulation efficacy for patients with Parkinson's disease. Brain 2010;133:2007–21. https://doi.org/10.1093/brain/awq144.